Molecular and Nano-engineering with iron, ruthenium and carbon: Hybrid structures for sensing

Geest, E.P. van

Chapter 4

Polymer-coated graphene-based gas sensors: chemical fingerprinting by simultaneous sensing

Graphene is very suitable for building electronic sensors, for example to detect biomarkers, yet it is challenging to obtain clean, polymer-free graphene, as often polymer residues remain on the graphene sheet after polymer-assisted transfer and polymer removal. Here we show that graphene-based transistors can keep the intact transfer polymer layer, to yield sensitive sensors for the detection of various chemicals in the gas phase. In such sensors, the polymer layer functions as the sensitizing material, and it protects the graphene sheet, which reduces the noise of the device significantly. Using such systems, chemical vapors were electrically sensed down to the ppm level, and components of mixtures (methanol/ethanol and ethanol/water) could be quantified with these sensors. Yet, single polymer-coated sensors were not selective. Combining three sensors with three different polymer coatings yielded chemical fingerprint (CF) arrays with which the chemical fingerprint of 42 different chemical vapors were obtained, based on the combined response of the three individual sensors. Such "chemical fingerprinting" could be used for identification of chemical vapors: the CF array data could indeed be used to feed supervised machine learning algorithms for compound classification and identification with high accuracy. Polymer-coated graphene sensors can thus sense and identify chemical vapors at low concentrations through common electrical readout.

E.P. van Geest, H. de Bruijn, X. Liu, G. van Westen, S. Bonnet, and G.F. Schneider, manuscript in preparation. Patent application filed.

4.1. Introduction

In medical clinics, detection of biomarkers plays an important role as a guide for early and reliable diagnoses.[1] The importance of biomarkers is in the deviations of their natural levels, an indication that the human body might be suffering from an illness; biomarker detection is in fact mentioned for the diagnosis of various diseases, and molecular changes in biomarkers and their relationship to illnesses have been widely researched.[2] Breath analysis has been mentioned as a screening method to track lung cancer, for instance.[3] Common methods to analyze a patient's breath range from small and low-cost sensors, *i.e.* solid-state (metal oxide) gas sensors that are useful for continuous measuring of known compounds, to advanced techniques based on optical spectroscopy, (high resolution) mass spectroscopy and gas chromatography for example, which have the advantage that they can be used to identify unknown compounds for untargeted breath analysis.[4, 5] An important disadvantage of these advanced techniques is that they often require expensive equipment and trained personnel, which is too expensive if the analysis is to be performed on a large group of subjects with screening and risk assessment in mind. On the other hand, solid-state sensors typically suffer from poor selectivity, which is sometimes resolved by using sensor arrays in e-noses for combinational selectivity through pattern recognition.[5] Ideally, devices for biosensing should detect biomarkers preferably without any pretreatment of the breath sample, meaning they need to measure in the low ppm to ppt range (the concentration range of common biomarkers in breath[6]), should be chemically selective, and should be cheap and easy to use.

Graphene has been mentioned as a good candidate to be used in sensing devices that can fulfil these requirements.[7, 8] Yet, to unlock its sensing potential, graphene needs to be functionalized: a molecule or (nano)particle has to be introduced on its surface, which provides graphene-based sensors with sensitivity and selectivity.[9] To be functionalized, graphene is commonly transferred to a substrate by the aid of a transfer polymer.[10] This polymer usually has to be removed after transfer, typically by dissolving it with acetone, to expose the graphene surface for further functionalization. However, solubilizing the polymer is not a clean procedure; often residues from the transfer polymer remain.[11] These residues can strongly influence the electrical and thermal properties of graphene, as well as the performance of graphene-based sensors.[12,

[13] On the other hand, the transfer polymer itself and the residues can also act as the functionalization itself. Indeed, sensors with poly(methyl methacrylate) (PMMA) residues on the graphene sheet have been reported to respond to a variety of chemical species (for example water, nonanal, and octanoic acid vapors), while cleaned devices did not respond to these vapors. Atomic force microscopy showed that these residues were randomly distributed on the graphene sheet.[13] In principle the random, uncontrolled deposition of polymer residues on graphene complicate reproducibility of graphene-based sensing devices, as the amount and chemical nature of the residues can vary strongly between sensors.

In this work, the transfer polymer was left intact on the graphene sensor to circumvent this reproducibility issue, and to obtain a homogenous functional layer which is the sensitizing component of the graphene sensor. An additional advantage of leaving the transfer polymer intact is that it physically protects the graphene sheet, thereby reducing electronic noise. Polymer-coated sensors were hence made that respond reliably to a wide range of vapors, as the polymer has limited molecular-based selectivity (as opposed to streptavidin-based biotin and aptamer sensors for example, which are selective to single targets, their biological binding partner[8]). However, different transfer polymers do give rise to different responses; by making arrays of three sensors with different transfer polymers, it was possible to generate array sensors that showed excellent chemical selectivity. The combined information of the multiple sensors creates a unique profile of sensing responses, in other words a chemical fingerprint for each chemical species. The presence of a certain chemical species in an unknown sample could then be deduced using this fingerprint, *i.e.* through algorithmic deconvolution of the signal and machined learning to obtain qualitative (the chemical identities) and quantitative information about the chemical species that was sensed (see Figure 4.1).

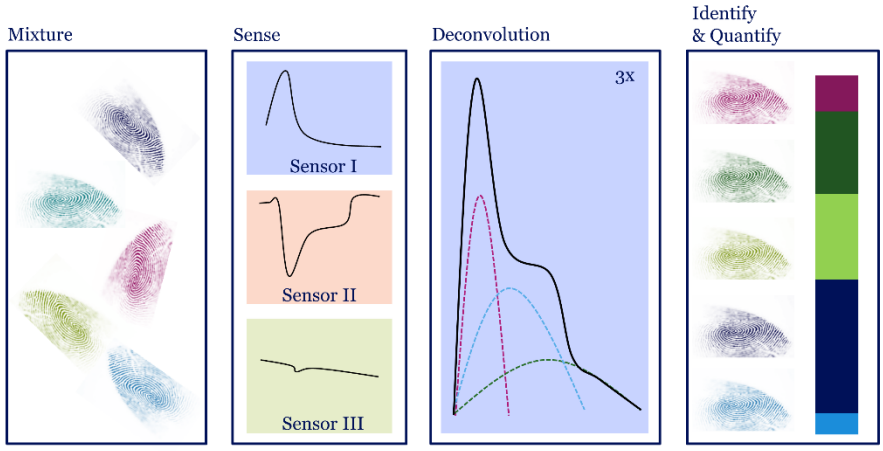

Figure 4.1: Schematic workflow of identification of chemical vapors with polymer-coated graphene-based sensors using the chemical fingerprint of the vapors. When a mixture of unknown composition is sensed by an array of sensors, the responses of these sensors could be used for the deconvolution of the sensing response by using the chemical fingerprints, *i.e.* the response of chemical vapors to the same sensors, to identify and quantify the individual components of the mixture.

4.2. Results and Discussion

4.2.1. Fabrication of polymer-coated sensors

A cleaned silicon wafer of 10 x 20 mm (see Figure 4.2A, I) was exposed to oxygen plasma and coated with masking tape that had cutouts for the electrodes of the sensor (II). Electrodes were produced using Tollens' reagent yielding a layer of metallic silver (III). After 15 minutes at room temperature, the silvering solution was removed and the wafer was rinsed with water (IV). Next, the mask was removed and the wafer was sonicated for 5 minutes in acetone and rinsed with acetone, ultrapure water, and 2-propanol to remove any remaining silver particles (V). Graphene was then transferred using polymer-assisted transfer (VI). This transfer polymer was not removed after graphene transfer. Finally, copper wires were connected to the silver electrodes and to the silicon back side of the wafer, to finish the device (for a photograph of a finished device, see Figure S4.1). Importantly, the devices had six electrodes A to F, to eliminate contact resistance by applying the current I_{AF} on the outer electrodes, while measuring the potential between the inner electrodes B & C and D & E. By installing four inner electrodes (instead of two, which is conventional in 4-terminal sensing), two transistors could be measured simultaneously, denoted MEAS(urement) (V_{BC}) and REF(erence) (V_{DE}), to make sure a sensing response is a true signal and not an

artefact in the measurement (see Figure 4.2B). Notably, for devices with polymer-coated graphene, the resistivity values of MEAS and REF were often very similar (in the range of hundreds of ohms). In contrast, for devices where graphene was exposed by removing the transfer polymer resistivity values were typically higher (kilo-ohms) and differed more strongly between MEAS and REF as compared to the polymer-coated devices, indicating that the exposed graphene devices were more defected; furthermore, their electrical noise was significantly higher.

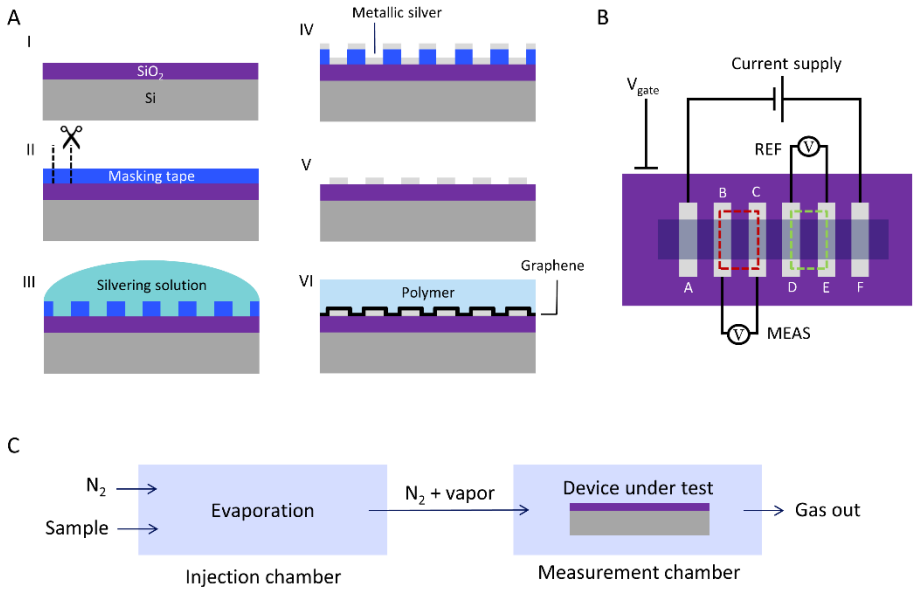

Figure 4.2: Polymer-coated sensors. A) Schematic representation (side view) of the fabrication process for a polymer-coated graphene-based sensor, step by step. A silicon wafer was cleaned and treated with O_2 plasma (I) and coated with pre-shaped masking tape (II). Next, a silvering solution, *i.e.* Tollen's reagent, was placed on the masked wafer (III) to deposit a layer of metallic silver (IV). Then, the masking tape was removed and the wafer was sonicated (V), after which polymer coated-graphene was transferred without removing the polymer (VI), and finally the electrodes A to F were connected to finish the device. B) Schematic top view of a typical device with the reference and measurement transistors (MEAS and REF, red and green rectangle, respectively). The gate voltage was set to 0 V for all devices. C) Gas measurement setup (side view), consisting of an injection chamber where volatile samples were injected with a syringe and evaporated; the vapor was then carried by a nitrogen flow to the measurement chamber containing the sensor.

4.2.2. A polymer layer for protection and reproducibility

To study in the first place if the polymer-coated sensors could give reproducible responses to chemical vapors, initially a PMMA coating was used for vapor detection experiments. For some sensors, PMMA was dissolved with acetone to

check the influence of the polymer on sensing. Devices with or without PMMA were placed in the measurement chamber that was connected to a separate injection chamber. Volatile samples were injected manually in the injection chamber (typically 10 µl per injection), and the vapors were carried to the measurement chamber by a nitrogen flow (see Figure 4.2C, for a photograph, see Figure S4.2). In a first stage, 15 volatile compounds were tested to make sure the injected volume evaporated and passed the measurement chamber within a period of 500 s, which was used as the time between two consecutive injections. The resistance R of MEAS and REF graphene sheets were measured continuously.

The transfer polymer PMMA had a large impact on the behavior of the sensors. In the plot of resistivity *vs.* time of the PMMA-coated device, the response peaks that appeared, for example when 4 injections of acetone were introduced in the injection chamber, were very similar in shape and intensity. On the other hand, when the PMMA layer was absent, no response to acetone could be observed at all (see Figure 4.3A). The large difference between PMMA-coated devices and PMMA-free devices highlighted the protective role of the polymer for the graphene sensors, and its critical role for gas sensing. In fact, PMMA-coated graphene sensors responded to a large number of the compounds that were injected (see Table S4.1). However, the time responses of the resistance to the various compounds injected were often different (see Figure S4.3). To compare vapor responses, the sheet resistivity ρ ($\rho = R \times w / l$, where w and l are the width and the length of the sheet) was normalized with respect to the resistivity value at the start of the measurement ($\rho_{t=0}$) to obtain ρ_{norm} (where $\rho_{norm} = \rho/\rho_{t=0} \times 100$). The curve ρ_{norm} *vs.* time was integrated over a range of 500 s with a linear baseline correction, starting from the moment of injection, to obtain the peak area A_{norm} (see Figure 4.3B). Most of the times, the ρ *vs.* time curves obtained for a series of multiple injections of the same compound were reproducible (water was an exception here, as discussed in section 4.2.3). The peak areas A_{norm} were reproducible as well for all compounds except water, as indicated by the small error bars on the average peak area (see Figure 4.3C and Table S4.1), which is required to identify the chemical vapors through analyzing the sensor response.

In fact, some compounds could already be identified by the value of the peak area for PMMA-coated devices. Acetonitrile, for example, was the only compound of this set that gave a negative peak area. Interestingly, the peak areas for the alcohol series (methanol, ethanol, 1-propanol, and 2-propanol) which are chemically very

similar, strongly differed, showing that these devices can reliably differentiate between chemically similar compounds. Similarly, different aromatic species a showed distinct responses: pyridine for example gave a strong response, while toluene, anisole and benzonitrile gave low responses. On the other hand, some compounds could not be detected as no peak in *R vs.* time appeared. This is the case for diethyl ether and pentane for example. We believe that these differences in response of the vapors are due to the different interactions of the sensed molecules with the PMMA layer as the vapor is absorbed by the layer, leading to specific conformational changes in the PMMA layer. Graphene is sensitive to such changes, and hence the electronic properties of graphene change, giving a sensing response. Over time, the nitrogen flow desorbs the molecule, and the resistivity returns to the baseline.

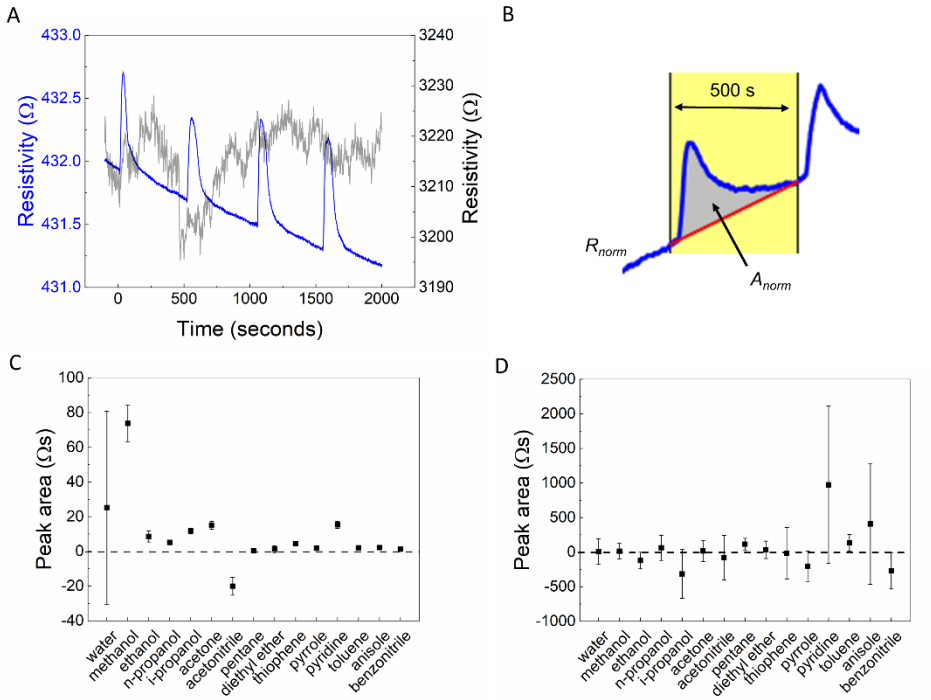

Figure 4.3: PMMA-graphene based devices responded to manually injected chemical vapors. A) Resistivity ρ *vs.* time for a typical PMMA-coated (blue) and PMMA-free (grey) graphene device. Acetone was injected 4 times, 10 µl per injection, with the first injection at t = 0 s, then at intervals of 500 s. B) Integration of the peak area from the normalized resistivity ρ_{norm} over 500 s, yielded the peak area, A_{norm}. C-D) Peak area (A_{norm}), averaged for each compound, for a PMMA coated device (C) and PMMA-free graphene device (D). Each data point represents 4 sequential injections of 10 µl of the same compound with 500 s between each injection, except acetone, which was injected 6 times. The data that was used to construct C and D is shown in Table S4.1.

Notably, the response reproducibility that was obtained with PMMA-coated graphene devices was not achieved with exposed graphene devices, as the error bars in the peak intensities for the different compounds for these devices were much larger than the errors for PMMA-coated devices (see Figure 4.3D and Table S4.1). Thus, the reproducibility of the responses to a large set of compounds was strongly enhanced by the presence of the PMMA coating, and the sensor could differentiate between various compounds, even if they are chemically similar.

4.2.3. Water saturation, and how to overcome saturation

The response of PMMA-coated devices appeared to be not reproducible for water. When water was injected, the device with PMMA coating quickly saturated with water, as shown by a large decrease of $\Delta\rho$ for the 2nd, 3rd and 4th injection as compared to the 1st injection, see Figure 4.4A. The saturation and long recovery time for water (>500 s) was problematic for these sensors, yet could be overcome by subsequent injections of acetonitrile. After saturation of a sensor by injecting water (4 x 10 μl), the resistivity of the sensor could be decreased by injecting acetonitrile (4 x 10 μl), back to values that were even below the initial value (*i.e.* before the first water injection, see Figure 4.4A). Alternating injections of water and acetonitrile showed that the sensitivity of the sensor to water was restored every time after an acetonitrile injection, as indicated by the positive peak area for water after an injection of acetonitrile, in contrast to the negative peak areas for sequential injections of water (see Figure 4.4B and C). Importantly, the error bars on the average peak area for water were severely reduced by following each water injection with an acetonitrile injection instead of another water injection (see Figure 4.4D), showing that saturation of the sensor with water could be cleared by flushing the sensor with acetonitrile. Acetonitrile thus functioned as a "reset button" for PMMA-coated sensors after saturation with water.

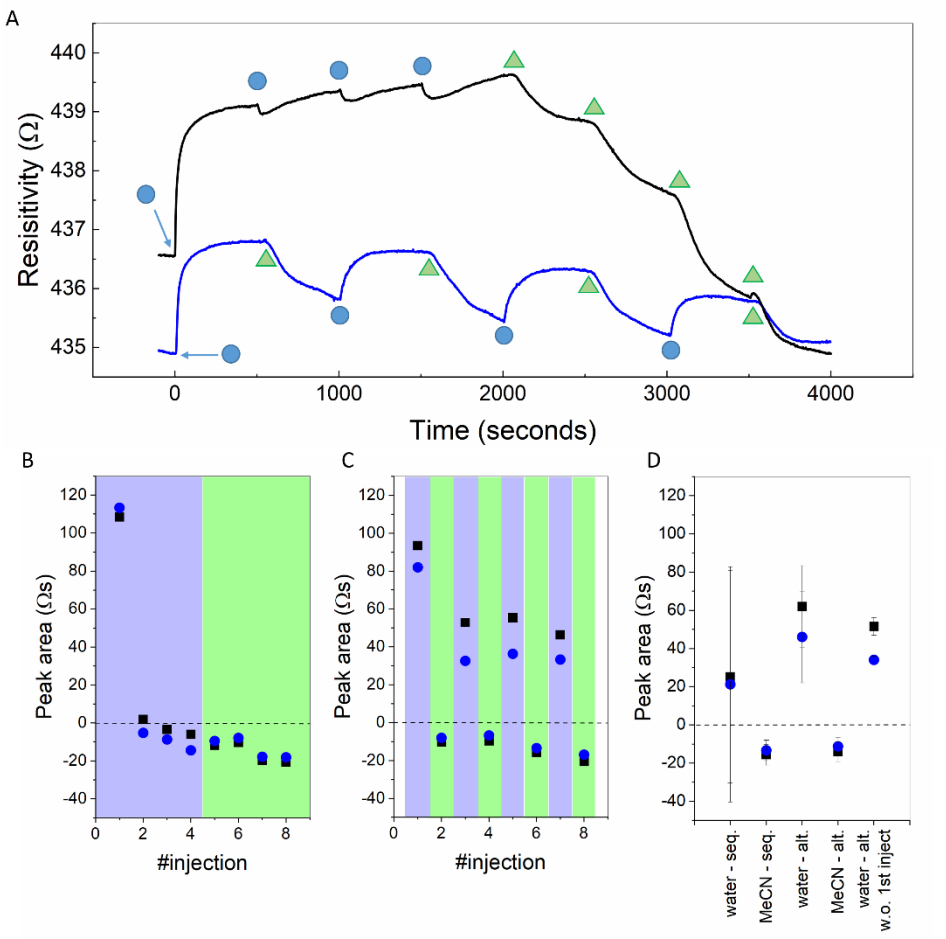

Figure 4.4: Acetonitrile as a "reset button" for PMMA-coated sensor saturation by water. A) Resistivity ρ *vs.* time for sequential and alternating injections (black and blue line, respectively) of water and acetonitrile (blue circles and green triangles, respectively), 10 µl per injection. B-C) Peak area for sequential (B) and alternating (C) injection of water and acetonitrile for MEAS (V_{BC}, blue) and REF (V_{DE}, black), light blue box = water, light green box = acetonitrile, 10 µl per injection. D) Averages of the peak area for water and acetonitrile when injected sequentially or alternating (for the last input, the data from the first water injection was during alternated injection was excluded).

4.2.4. Detection limit & component quantification in mixtures

To evaluate the sensing performance and limitations of the PMMA-coated devices, methanol was used either pure or in mixtures, in particular because the sensor gave strong responses on exposure to methanol. First, we studied how the sensor responded to lower amounts of methanol by lowering the injected volume. Methanol could be detected with injected volumes in the range of 5 to 0.1 µl (see

Figure 4.5A). Moreover, the peak area of the response decreased as the amount methanol was lowered, which followed a linear trend (Figure 4.5B). The peak area was thus directly related to the amount of the sample that was injected, which is useful for compound quantification with PMMA-coated graphene sensors.

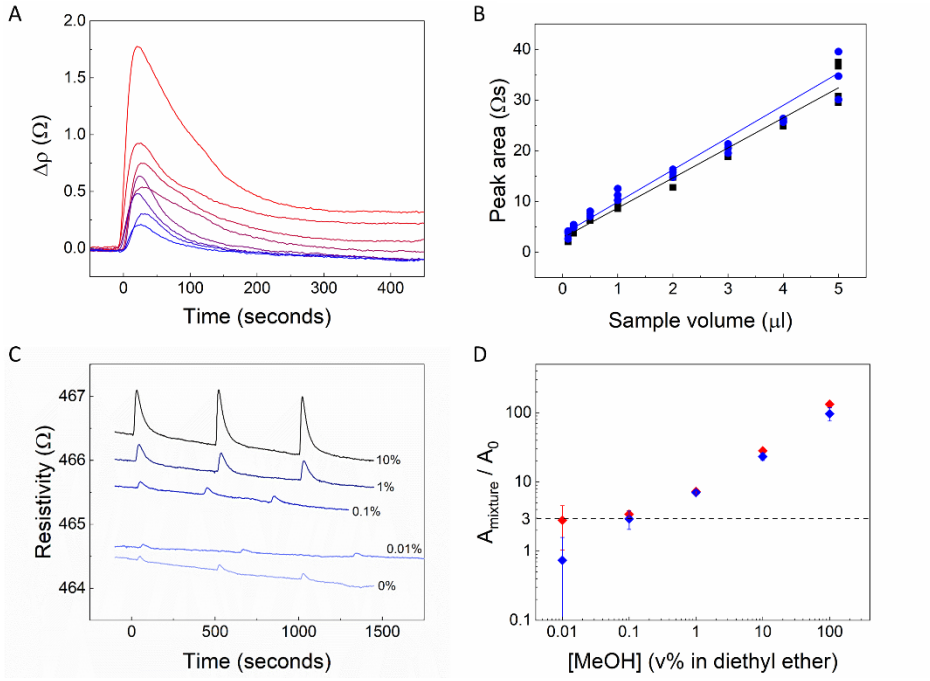

Figure 4.5: Detection limit for methanol and component quantification in mixtures for PMMA-coated devices. A) Resistivity change $\Delta\rho$ of a PMMA-coated graphene sensor (MEAS, V_{BC}) upon injection of decreasing amounts of pure methanol (from red to blue: 5, 4, 3, 2, 1, 0.5, 0.2, and 0.1 µl). B) Peak area A_{norm} from normalized resistivity *vs.* volume of methanol injection, MEAS (blue, $R^2 = 0.9814$) and REF (V_{DE}, black, $R^2 = 0.971$). C) Resistivity (MEAS) upon multiple injections (10 µl per injection) of methanol/ether mixtures, the percentage indicates the volumetric concentration of methanol. D) Peak area A_{norm} of a methanol/ether mixture relative to the peak area for pure ether, $A_{mixture}/A_0$, *vs.* v% methanol in diethyl ether for MEAS (blue) and REF (red). When $A_{mixture}/A_0 > 3$, (indicated by the dashed line), methanol is considered as "detected".

To find the detection limit of these sensors for methanol, solutions of methanol in diethyl ether (0, 0.01, 0.1, 1, 10 and 100v% methanol) were injected, using diethyl ether as an "inert" carrier solvent here, as ether gave only a very small response on the sensor (see Figure 4.5C and Figure S4.4). Quantification of the amount of methanol (by peak area) in ether was done using a sensing threshold of $A_{mixture}/A_0 \geq 3$, where $A_{mixture}$ is the peak area of methanol solution in diethyl ether and A_0 is the peak area of pure diethyl ether. The factor 3 was chosen, as

signal to noise usually has to be higher than 3 to claim the detection of a species. The background peak from diethyl ether, here functioning as a carrier solvent, was considered as the noise in this experiment. The signal will not be affected significantly with decreasing amount of diethyl ether in the mixture, so we can assume this contribution as continuous throughout the experiment. Using these criteria, methanol presence in the solutions could be detected down to 0.1v% methanol in 10 μl injections (see Figure 4.5D), which corresponds to 0.01 μl of methanol. With the system volume estimated to be 0.5 l, the detection limit of methanol for these sensors was estimated to be 6 ppm. The responses from PMMA-coated graphene devices can thus be used to determine the composition of methanol/ether mixtures and to find the detection limit of the sensor.

To further analyze the sensor response to mixtures of chemicals, we investigated first mixtures of ethanol and methanol, then mixtures of water and ethanol. A series of different concentrations of methanol in ethanol (0 to 100v%, injections of 1 μl, see Figure 4.6A) showed a strong linear relationship between the peak area of the normalized resistivity *vs.* methanol content (Figure 4.6B). Due to the specific response of the PMMA sensors with water, quantification of the ethanol content in water was not determined by considering the peak area of the resistivity traces (Figure 4.6C), but by analyzing the full-width-half-maximum (FWHM) of the resistivity trace (after linear baseline subtraction). We found a linear relationship between the FWHM, an indication of the tail of the peak, and concentration of water in ethanol (Figure 4.6D): the shorter the tail of the peak indicated by a low FWHM value, the higher the ethanol content, likely because ethanol was easier to be removed from the sensor than water. This linear relationship may be used to determine the ethanol content in water. The PMMA coated sensor can thus be used for quantification of the composition of (binary) mixtures of chemically similar compounds.

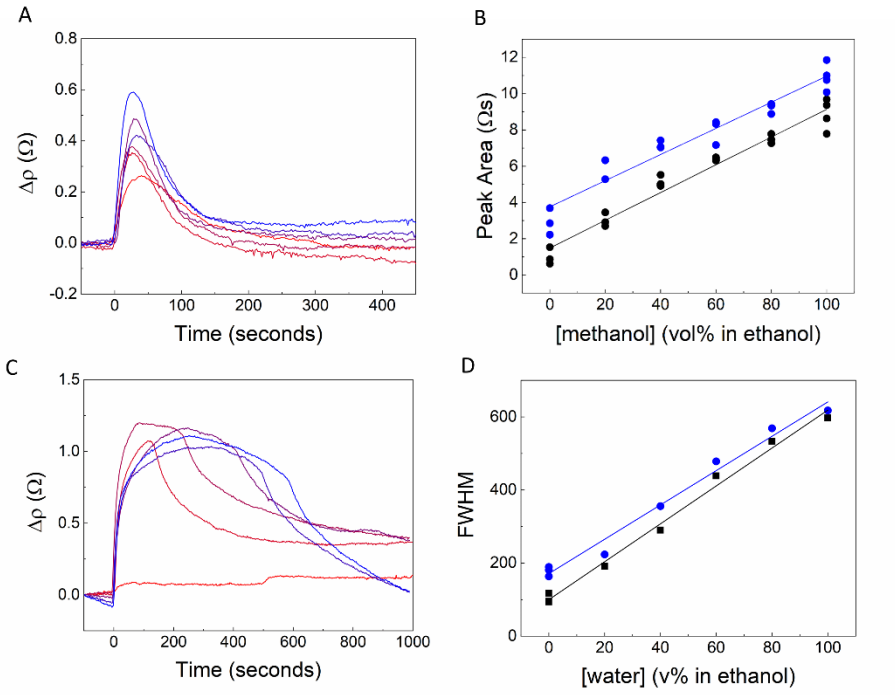

Figure 4.6: Component determination of mixtures with PMMA-coated graphene devices. A) Resistivity change $\Delta\rho$ upon injection of solutions of methanol in ethanol (from red to blue: 0, 20, 40, 60, 80, and 100% methanol, injections of 1 µl, MEAS, V_{BC}). B) Peak area A_{norm} *vs.* v% methanol in an ethanol solution showed a linear relationship, MEAS (blue, $R^2 = 0.9206$) and REF (V_{DE}, black, $R^2 = 0.9602$). C) Resistivity change $\Delta\rho$ upon injection of solutions of water in ethanol (from red to blue: 0, 20, 40, 60, 80, and 100v% water in ethanol, injections of 1 µl, MEAS). NB: 0% water was injected twice, at 0 s and 500 s. D) Full-width half maximum of the peaks (after linear baseline correction, interval between injections = 1000 s) in normalized resistivity *vs.* v% water. A clear linear relationship was observed for MEAS (blue, $R^2 = 0.9918$) and REF (black, $R^2 = 0.9838$).

Yet, to identify unknown compounds, and more importantly mixtures of unknown compounds, the chemical selectivity of PMMA-coated sensor was too low. To tackle this problem, we investigated other polymer coatings, as we realized that by producing an array of sensors with different polymer coatings, we may reconstruct chemical selectivity in sensing by analyzing the "fingerprint" response of an array of sensors.

4.3. Chemical fingerprint (CF) vapor sensors

4.3.1. A sensor array with different polymer coatings

To study whether the chemical composition of the polymer influences the sensing response of the graphene sensor to different chemicals, two additional polymer

coatings were used to build the graphene sensors, *i.e.* Nafion® 117 and cellulose acetate butyrate (CAB), to create identical sensors but with coatings that are chemically different in nature. Then, three graphene sensors with the three different polymer coatings were placed in an sensor array, in a single chamber, so the resistance of the three sensors could be monitored simultaneously while they were exposed to the same chemical vapors. We hypothesized that each sensor in the array will give a poorly specific, but different response to vapors compared to the two other sensors as their coatings are chemically different, and that the combination of these different responses may be used to construct a "chemical fingerprint" of the vapor that was in the sensor space, to afford high chemical specificity.

Sensor arrays built for this purpose, denoted below as "chemical fingerprint (CF) arrays", were made using the same techniques as those described for the PMMA-coated sensors above (see section 4.2.1). First, a mother chip was produced, *i.e.* a silicon wafer (1 x 4 cm) with two silver electrodes stretching over the length of the wafer, bridged by a sheet of graphene coated with PMMA, Nafion® 117 or CAB (which were used as the transfer polymer). Next, daughter chips were created by cutting the mother wafer perpendicular to the two electrodes (see Figure 4.7A, Figure S4.5 and supplementary text). Wiring the daughter chips yielded single CF sensors (Figure S4.6) to be implemented in the CF array. The resulting CF sensors were small in width (2 to 3 mm) to ensure that they fitted in a sample chamber that was sufficiently small to avoid vapor dilution. Gas-tight sensor caps were fabricated that fitted on a cut gas chromatography (GC) column (Figure S4.7). Finally, three CF sensors (one of each of the PMMA, Nafion® 117, and CAB coated sensors), were placed in a single CF array tube, which was capped and sealed (Figure S4.8) to finish the CF array (see Figure 4.7B). For a photograph of a finished CF array, see Figure S4.9.

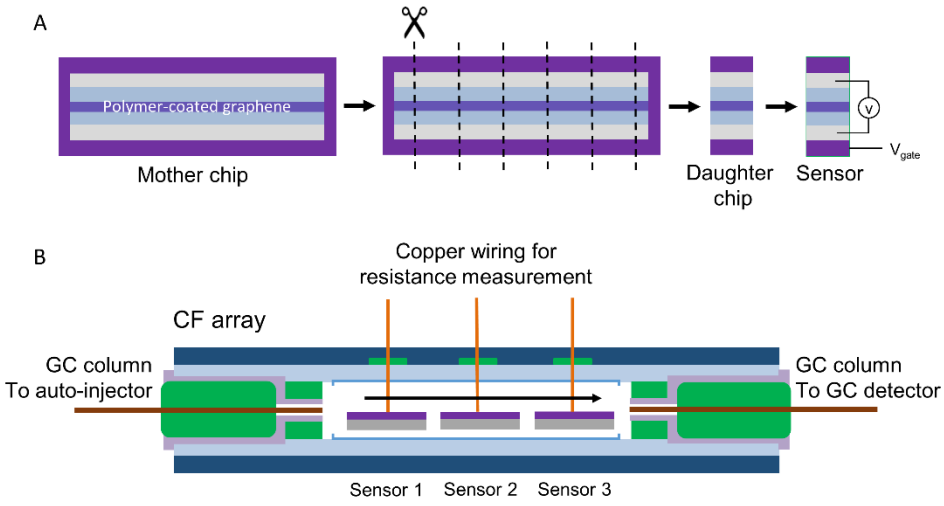

Figure 4.7: Chemical fingerprint array. A) Fabrication, in short, of a CF sensor. A mother chip with two electrodes stretching over the whole length of the surface, bridged by a polymer-coated graphene sheet, was cut to produce identical daughter chips, which were wired to create fabricate individual CF sensors with similar response. B) Schematic representation of a chemical fingerprint (CF) array, built with three CF sensors, each of which is coated with a different polymer on graphene. The three sensors were assembled in a gas-tight, multi-walled sensor tube that was connected to a GC column for automated chemical vapor injection. Arrow indicates flow direction.

4.3.2. Continuous CF array measurement with auto-injection

In order to enable automated, continuous measurements in presence of many different chemicals, CF arrays were connected inside the oven of a GC system. The GC allowed to control the temperature of the sensors (typically set to 30 °C), ensured a steady gas flow of the carrier gas (helium), and most importantly, allowed the use of the auto-sampler connected to the GC. The advantage of the auto-sampler was that all compounds were injected multiple times in the same manner, bypassing human errors, for example variations in volume and temperature of the injected species. The CF array was attached to the column of the GC (that was cut ~30 cm away from the auto-injection port of the GC) by inserting the cut ends of the column in the caps of the CF array (see Figure S4.10). This connection was gas-tight, as the hole in the caps through which the column ends were inserted were smaller in diameter than the column itself, and the cap material was elastic, which sealed the connection between the cap and the column. The sample injector was set to 300 °C to ensure complete evaporation of the injected species. Samples were injected multiple times in volumes of 1 µl at a split ratio of 1:40, meaning only 1/40th of the 1 µl sample was introduced on the

GC column and thus reached the sensor; the remainder was discarded by the GC apparatus. CF arrays were thus operated under standard GC conditions.

4.3.3. Establishing the fingerprints for 42 different chemical vapors

The resistance of the sensors in a CF array was monitored continuously over several days, while the GC auto-injector introduced the samples automatically and repeatedly with a time interval of 830 s between two consecutive injections. In total, 42 different compounds (see Table S4.2) were introduced 4 times each to the CF array, to build a database of chemical fingerprints of these compounds obtained from the CF array sensors, and study the reproducibility of the signal. The obtained resistance *R vs.* time traces were different for the three individual sensors in each array coated with the three different polymers. For 38 of the 42 compounds, a significant peak was found in at least one of the sensors; only pentane, cyclopentane, 1-pentene and 1-chlorohexane did not show response on any of the sensors of the CF array (see Figure S4.11). Notably, CAB-coated sensors showed a higher signal-to-noise ratio and shorter recovery time than PMMA- or Nafion® 117-coated sensors, for reasons that are not obvious to us.

To investigate if the position of the compounds in the series of injections introduced in the array sensors influenced the response of the sensor to these compounds, the measurement with the same compound database was repeated on the same CF array, while the injection sequence was randomized. The response of the CF sensors appeared the same to all compounds, regardless of the injection sequence. The order of introducing compounds to the sensor thus seemed to have no effect on the response of the CF array (see Figure S4.12).

The two essential characteristics of the chemical fingerprint of each injected compound were the shapes of the curves of the R_{norm} *vs.* time traces for all three polymers, where $R_{norm} = R / R_{t=0} \times 100\%$, as well as the 3 integrated areas A_{norm} under these curves, as explained above for PMMA (see Figure 4.8 and Figure S4.13). Importantly, the error bars were small for the average value of A_{norm} for each compound on each type of polymer coating, indicating the responses of sensors to the compounds were reliable (see Table S4.3). This was true unless saturation occurred, similar to the saturation of PMMA-coated devices by water as described in section 4.2.3, which was the case for pyrrolidine and piperidine for example. Moreover, the peak area values that were obtained from three differently coated graphene sensors for a typical compound was not the same for the different

sensors, showing that the response behavior is determined by the polymer coating type, and adding sensors with a different polymer coating to the array provides additional data for a chemical fingerprint. Importantly, the peak area values that were obtained also differed between different compounds that were introduced. The CF array was thus able to discriminate between the different injected compounds, which is required for the precise identification of the chemical vapor flowing above the CF array sensor.

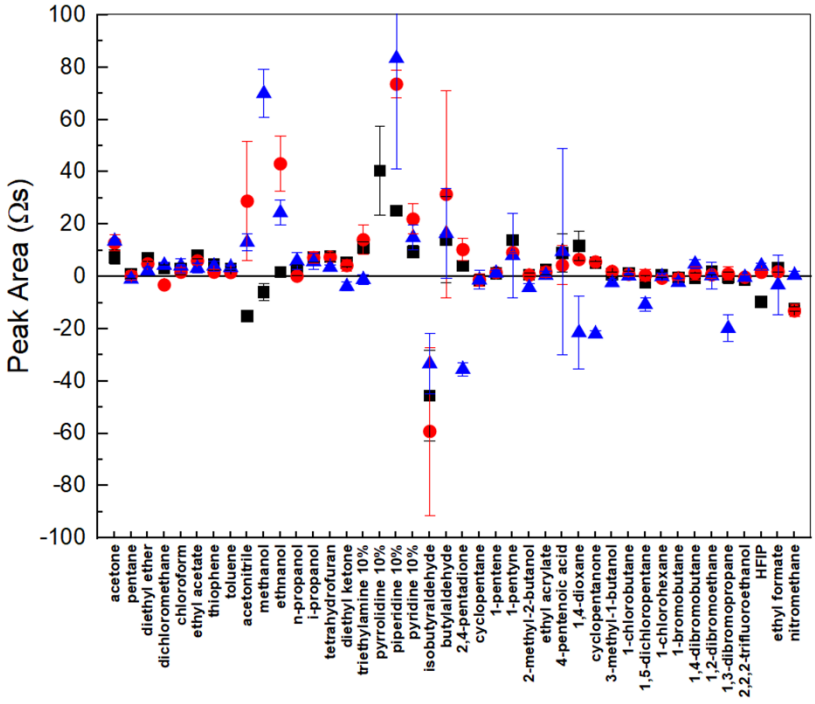

Figure 4.8: Chemical fingerprint of a series of 42 different chemicals, based on the average peak area, A_{norm}, obtained from normalized resistivity data (R/R_0 x 100) on CF array **1**, containing three graphene sensors coated with PMMA, Nafion® 117, or CAB (black squares, red circles and blue triangles, respectively). The peak areas shown are averages obtained for 4 individual injections (1 µl, split ratio = 1:40) for each species, except for acetone, which is an average of 6 injections. HFIP = 1,1,1,3,3,3-hexafluoro-2-propanol. Notably, the peak areas from certain compounds were out of range for the scale of this graph. The full graph and data that was used to construct the graph are shown in the supplementary information (Figure S4.13 and Table S4.3).

From the obtained data with one CF array, some chemicals could be already identified by a simple look at the raw data. For example, nitromethane could be recognized from the strong response on all three CF sensors and typical profile on the PMMA sensor (first a sharp decrease, followed by a bell-shaped peak, see

Figure S4.14), as well as 1,1,1,3,3,3-hexafluoro-2-propanol (HFIP), which could be recognized by the strong response and typical profile on the three sensors (for example, on the PMMA and Nafion® 117 coated sensors, HFIP showed first an increase, then shortly a slow decrease, then a sharp drop after 50 – 100 seconds, see Figure S4.15). Visual inspection of the raw data can thus already be used to identify some of the chemical species, showing that the CF arrays can be more useful for compound identification than a single graphene sensor with a single polymer coating. Yet, we hypothesized supervised learning could be a far more powerful tool for compound identification from the CF array datasets than the naked eye.

4.3.4. Machine learning for compound identification

The CF array data of 34 out of 42 compounds were found suitable for analysis by supervised machine learning using the criterion that a compound must give a response to all three sensors in the array (see Table S4.3). In total, we tested three different batches of data (run I, II and III), in which there were four samples for each compound. Batch I and III were merged and used as the training set, while batch II was used as an independent test set. After removing the noise and blank samples, there were 238 and 110 samples in the training and test set, respectively. For each sample, 10 features were extracted from sensor data as is illustrated in Figure 4.9A, including maximum and minimum values of resistance R_1 and R_2, the time points of the maximum and minimum of resistance t_2 and t_4, the largest and smallest slope S_1 and S_2, the time points of largest and smallest slope t_1 and t_4, and the area of response process A_1 and area of recovery process A_2.

Subsequently, supervised machine learning models were constructed for multi-label classification, which take these 10 features as the input and categories of molecules as output, respectively. Four algorithms were benchmarked for model construction: Random Forest (RF),[14] K-Nearest Neighbours (KNN),[15] Naïve Bayesian (NB),[16] and Support Vector Machines (SVM).[17] The RF, KNN, NB and SMV models were implemented through Scikit-Learn. In RF, the number of trees was set as 1000 and split criterion was "gini". In KNN, the number of neighbours was set as 3. In SVM, a radial basis function (RBF) kernel was used and the parameter space of C (the cost of misclassification parameter) and γ (the free parameter of the RBF kernel) were set as $[2^{-5}, 2^{15}]$ and $[2^{-15}, 2^{5}]$, respectively.

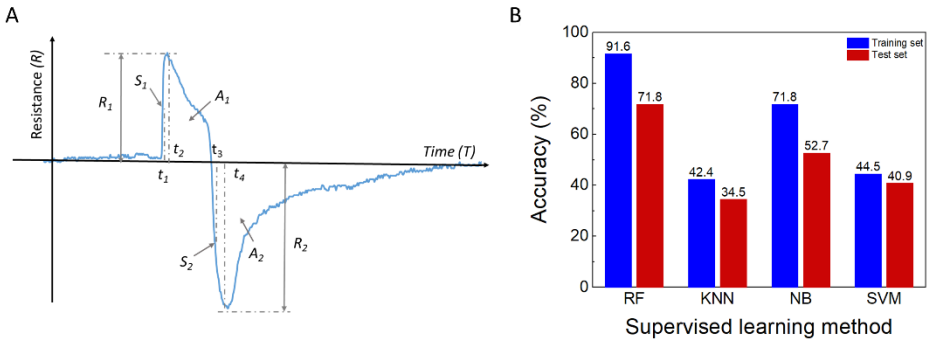

Figure 4.9: Data analysis by supervised learning. A) Features were extracted from the CF array data of one sample, including maximum of resistance (R_1), the largest slope (S_1), the time point of largest slope (t_1), the time point of maximum of resistance ($t1$), the area of response process (A_1), minimum of resistance (R_1), the smallest slope (S_2), the time point of smallest slope (t_3), the time point of minimum of resistance (t_4) and the area of recovery process (A_2). B) Performance comparison between different supervised learning methods on both training set with cross validation and test set with independent test, respectively.

A principal component analysis (PCA)[18] was employed on the feature data, shown as 3D plot in Figure S4.16, and we found that almost all of the samples from the same compound were located closely. However, the compounds could not be clustered into distinct groups. Moreover, the PCA could not reflect an apparent relationship between the patterns of sensor data and properties of these molecules. The classification models, on the other hand, could accurately assign compound labels to the samples of our dataset (see Figure 4.9B). We found that among the different algorithms, the RF algorithm achieved the highest accuracy for compound classification on both the cross validation (training) and the independent (test) set, with accuracies of 91.6 and 71.8%, respectively. Using the RF algorithm, we could thus use the CF array data to classify and identify the different compounds that were introduced to the array with high accuracy.

We should emphasize here that this method does not require the development of radically different sensors, nor do they require complex, molecularly specific functional molecules or nanoparticles on the graphene sheet. The range of polymers which can be applied in such devices is enormous, making these sensors potentially cheap (polymers do not have to be designed specifically) and easy to fabricate. Here CF arrays made of 3 different sensors with 3 different polymers have been realized, but it is easy to imagine CF sensors with 4, 5, or 6 different polymers, which increases the chemical selectivity with each additional polymer.

4.4. Conclusions & Outlook

Our findings showed that leaving the transfer polymer layer on graphene in a graphene-based sensor unlocks their sensing capacity. PMMA-coated sensors responded to a wide range of chemical vapors, and the sensor response to these vapors varies with the chemical nature of the vapors. Devices coated with a polymer layer showed much higher signal-to-noise ratios than bare graphene ones, which we interpret as a protective function of the polymer layer. The PMMA-coated sensors reached the low ppm range for specific species, *i.e.* 6 ppm for methanol, while other compounds, like diethyl ether or pentane, could not be detected due to low response of the PMMA sensors. We demonstrated herein that such compounds can be used as inert carrier solvents for measuring low concentration of compounds that give a high response, such as methanol or water, respectively. Moreover, PMMA sensors also had the ability to distinguish between highly similar molecular compounds in mixtures, *i.e.* methanol and ethanol, or ethanol and water. Albeit these sensors saturated quickly in presence of water, acetonitrile was able to resolve this issue by quickly lowering the resistivity of the sensor after water saturation, thereby restoring the sensitivity of the sensor.

Although a single sensor with a single PMMA coating sensed different chemicals with some chemical selectivity, the selectivity was limited. To overcome this problem, we constructed chemical fingerprint arrays, which had three graphene sensors with three different polymer coatings that sensed the same chemical vapors by three simultaneous resistance measurements. These CF arrays were integrated in an auto-injection system, which allowed to measure the response of all three graphene sensors to 42 different chemical vapors: 38 of them triggered a response to at least one of the three sensors in the array. Through combining the information of the three sensors, the "chemical fingerprint" of each chemical vapor could be constructed, for the direct identification of the vapors. Using supervised machine learning techniques with the CF array data as input, compounds could indeed be classified and identified with high accuracy. Thus, with the CF array much higher selectivity was obtained than with single sensors. Moreover, the data from the CF array could be used to achieve excellent chemical recognition especially using machine learning, which paves the way to unlock the full potential of this CF array sensing technology.

4.5. References and Notes

[1] R. Mayeux, *NeuroRX* **2004**, *1*, 182.
[2] S. G. Coca, R. Yalavarthy, J. Concato, C. R. Parikh, *Kidney Int.* **2008**, *73*, 1008; B. Olsson, R. Lautner, U. Andreasson, A. Öhrfelt, E. Portelius, M. Bjerke, M. Hölttä, C. Rosén, C. Olsson, G. Strobel, E. Wu, K. Dakin, M. Petzold, K. Blennow, H. Zetterberg, *Lancet Neurol.* **2016**, *15*, 673; W. Whiteley, M.-C. Tseng, P. Sandercock, *Stroke* **2008**, *39*, 2902; N. L. Henry, D. F. Hayes, *Mol. Oncol.* **2012**, *6*, 140; R. Khoury, E. Ghossoub, *BIONPS* **2019**, *1*, 100005.
[3] R. Capuano, M. Santonico, G. Pennazza, S. Ghezzi, E. Martinelli, C. Roscioni, G. Lucantoni, G. Galluccio, R. Paolesse, C. Di Natale, A. D'Amico, *Sci. Rep.* **2015**, *5*, 16491; R. Einoch Amor, M. K. Nakhleh, O. Barash, H. Haick, *Eur. Respir. Rev.* **2019**, *28*, 190002.
[4] T. Bruderer, T. Gaisl, M. T. Gaugg, N. Nowak, B. Streckenbach, S. Müller, A. Moeller, M. Kohler, R. Zenobi, *Chem. Rev.* **2019**, *119*, 10803; O. Lawal, W. M. Ahmed, T. M. E. Nijsen, R. Goodacre, S. J. Fowler, *Metabolomics* **2017**, *13*, 110; K. H. Kim, S. A. Jahan, E. Kabir, *TrAC - Trend. Anal. Chem.* **2012**, *33*, 1; S. Scarlata, G. Pennazza, M. Santonico, C. Pedone, R. Antonelli Incalzi, *Expert Rev. Mol. Diagn.* **2015**, *15*, 933.
[5] C. Di Natale, R. Paolesse, E. Martinelli, R. Capuano, *Anal. Chim. Acta* **2014**, *824*, 1.
[6] M. Righettoni, A. Amann, S. E. Pratsinis, *Mater. Today* **2015**, *18*, 163.
[7] A. Nag, A. Mitra, S. C. Mukhopadhyay, *Sens. Actuator A Phys.* **2018**, *270*, 177; H. Huang, S. Su, N. Wu, H. Wan, S. Wan, H. Bi, L. Sun, *Front. Chem.* **2019**, *7*.
[8] W. Fu, L. Jiang, E. P. van Geest, L. M. C. Lima, G. F. Schneider, *Adv. Mater.* **2017**, *29*, 1603610.
[9] V. Georgakilas, M. Otyepka, A. B. Bourlinos, V. Chandra, N. Kim, K. C. Kemp, P. Hobza, R. Zboril, K. S. Kim, *Chem. Rev.* **2012**, *112*, 6156.
[10] J. Kang, D. Shin, S. Bae, B. H. Hong, *Nanoscale* **2012**, *4*, 5527; X. Li, Y. Zhu, W. Cai, M. Borysiak, B. Han, D. Chen, R. D. Piner, L. Colombo, R. S. Ruoff, *Nano Lett.* **2009**, *9*, 4359.
[11] M. Chen, R. C. Haddon, R. Yan, E. Bekyarova, *Materials Horizons* **2017**, *4*, 1054; T. Hallam, N. C. Berner, C. Yim, G. S. Duesberg, *Adv. Mater. Interfaces* **2014**, *1*, 1400115; Y. Chen, X.-L. Gong, J.-G. Gai, *Adv. Sci.* **2016**, *3*, 1500343.
[12] M. Ishigami, J. H. Chen, W. G. Cullen, M. S. Fuhrer, E. D. Williams, *Nano Lett.* **2007**, *7*, 1643; J. W. Suk, W. H. Lee, J. Lee, H. Chou, R. D. Piner, Y. Hao, D. Akinwande, R. S. Ruoff, *Nano Lett.* **2013**, *13*, 1462; A. Pirkle, J. Chan, A. Venugopal, D. Hinojos, C. W. Magnuson, S. McDonnell, L. Colombo, E. M. Vogel, R. S. Ruoff, R. M. Wallace, *Appl. Phys. Lett.* **2011**, *99*, 122108; J. H. Choi, J. Lee, M. Byeon, T. E. Hong, H. Park, C. Y. Lee, *ACS Appl. Nano Mater.* **2020**, *3*, 2257.
[13] Y. Dan, Y. Lu, N. J. Kybert, Z. Luo, A. T. C. Johnson, *Nano Lett.* **2009**, *9*, 1472.
[14] L. Breiman, *Mach. Learn.* **2001**, *45*, 5.
[15] N. S. Altman, *Am. Stat.* **1992**, *46*, 175.
[16] P. Domingos, M. Pazzani, *Mach. Learn.* **1997**, *29*, 103.
[17] C. Cortes, V. Vapnik, *Mach. Learn.* **1995**, *20*, 273.
[18] S. Wold, K. Esbensen, P. Geladi, *Chemom. Intell. Lab. Syst.* **1987**, *2*, 37.